REVISTA MATÉRIA V.30
ISSN 1517-7076 articles e20250214, 2025

Numerical and experimental evaluation of a small boat sandwich structure manufactured with natural fiber composite and Miriti wood

Mateus Fortes Carvalho[1], Mário Américo Xavier[1], Luis Paulo Brasil Souza[2], Roberto Tetsuo Fujiyama[1], Erb Ferreira Lins[3], Leonardo Dantas Rodrigues[1]

[1]Universidade Federal do Pará, Faculdade de Engenharia Mecânica. Belém, PA, Brasil.

[2]Pontifícia Universidade Católica do Rio de Janeiro, Departamento de Engenharia Mecânica. Rio de Janeiro, RJ, Brasil.

[3]Universidade Federal Rural de Pernambuco, Unidade Acadêmica do Cabo de Santo Agostinho. Cabo de Santo Agostinho, PE, Brasil.

e-mail: mateus14fortes@gmail.com, mamerico197@gmail.com, luisbrasil55@gmail.com, fujiyama@ufpa.br, erb.lins@ufrpe.br, leodr@ufpa.br

ABSTRACT

This work evaluates the technical viability of using green composites to build small boats, such as those used by riverine communities in the Amazon region. A 730 mm-long boat was constructed using a sandwich lamination technique. This miriti wood boat was coated with epoxy resin reinforced with two layers of unidirectional jute fabric on both the interior and exterior. The sandwich lamination provided benefits such as increased stiffness, impermeability, and a standardized production process. Fourteen strain gauges were installed on the boat's hull to measure strains in the key regions under various loads. The boat was experimentally tested using a bending test with bi-supported conditions. Additionally, a numerical model was developed using the finite element software ANSYS to simulate the same conditions as the experimental test. To enhance the accuracy of the numerical model, a code was developed using ANSYS Parametric Design Language to account for the anisotropic behavior of the jute composite. The numerical model was validated by comparing the experimentally measured strains with the calculated strains from the simulation.

Keywords: Green composites; Finite element method; Sandwich structures; Digital Image Correlation Technique; Small boats.

1. INTRODUCTION

Fluvial navigation is a distinct characteristic of transportation in the Amazon region, shaped by natural factors such as vast continental expanses, a challenging climate, and a terrain unsuitable for constructing highways and railroads. As a result, boat building is a regional necessity. Traditional boat-building methods originated from the expertise of Brazilian Indigenous communities, involving the selection of large-diameter tree trunks, which were hollowed out by burning and scraping until small boats took shape. These skills are still used today in riverine communities, where people demonstrate an innate talent for shipbuilding and fluvial navigation, as shown in Figure 1 [1].

Interest in natural fiber-reinforced composite materials has grown significantly, largely due to their sustainability. This is especially evident in green composites, which have been extensively studied over the past two decades, particularly in the nautical and automotive industries. Additionally, these materials offer numerous possibilities for environmentally friendly component design and manufacturing components. Composite materials are a class of materials with properties that surpass those of isotropic materials (such as metals, ceramics, and polymers) by offering high strength and low weight [2]. Natural fibers like Jute, Sisal, Cotton and Flax have a density in the range of 1400 to 1560 kg/m^3 and a Tensile strength around 350 to 940MPa [3], making them a good material for structural applications.

There are some articles in the literature studying the use of green composites in the manufacturing of marine components, including boat hulls. [4] presents an excellent overview of the evolution of the application of these materials in the naval industry. That work lists many types of natural fibers (including jute), comparing their properties with those of synthetic fibers commonly used in boat manufacturing. The study points not

Corresponding Author: Erb Ferreira Lins Received on 07/03/2025 Accepted on 25/08/2025

DOI: https://doi.org/10.1590/1517-7076-RMAT-2025-0214

Figure 1: Typical small boats used in amazon region [1].

only to the feasibility but also to the advantages of using green composites in the construction of small vessels, especially in regions with an abundance of natural fibers with good mechanical properties. The review shows that there is a significant lack of studies addressing the mechanical and environmental performances of eco-friendly structures.

In a recent review [5], various natural fibers and their combinations with hybrid composites are analyzed. Different techniques such as hand lay-up, compression molding, injection molding are discussed. The mechanical properties such as tensile strength and flexural strength are also presented as well as cost analysis, emphasizing the viability of natural fiber hybrids as sustainable alternatives in engineering applications

Although aluminum and synthetic fiber boats are viable options for marine transportation, they remain costly to manufacture. This reinforces the need to develop more affordable boats to meet the needs of riverine communities and overcome cost constraints. Some studies have explored composites made from polymeric resins and natural fibers abundantly available in the Amazon region such as bamboo, sisal, jute, and malva as in [6], which provides a comprehensive review of various works involving the use of sandwich structures made from natural fibers in marine applications, including the use of balsa wood as the core (a low-density wood similar to Miriti) which is used in present study. There are some studies on fracture behavior [7] and the feasibility of these materials in sectors like architecture and aviation, where they could replace metal alloys [8].

Additionally, several studies have investigated the fabrication of boats using natural fiber and hybrid composites. [7] investigates the potential of sugar palm fibers for use in hybrid composites, demonstrating enhanced tensile and impact properties. The study compares various fabrication techniques and finds that compression moulding is optimal for small boat production. In [2], a hybrid polyester composite using Curauá and E-glass fibers was developed. The hybrid showed mechanical properties comparable to fiberglass and significantly better than Curauá-only composites. It also proved to be an effective substitute for fiberglass in applications involving contact with water.

A natural fiber particularly abundant in northern Brazil is Miriti (Mauritia flexuosa). This is a palm tree native to the Amazon region which thrives in wetland and riverine areas and is valued for its high ecological and economic importance. Its wood is very light and soft, commonly used in traditional handicrafts, although it lacks resistance to bending (flexural) stresses.

In the present work, a boat prototype was constructed using composite materials through a sandwich lamination technique. A miriti boat was coated with epoxy resin reinforced with unidirectional jute fabric. This construction method offers several advantages, including increased stiffness, reduced weight, a more standardized production process, and improved impermeability. These benefits can support local communities in building lighter and safer boats. To the best of the authors' knowledge, this is the first study to apply this natural fiber in a real-world boatbuilding context. Also, the use of natural fibers in the production of boat can bring environmental benefits, since they are biodegradable and renewable, reducing the need for synthetic fiber that can harm ecosystems. The cost of Miriti wood and jute fiber is also very low when compared to other techniques used in boat construction.

We present the procedure for construction in section 2. This prototype was tested by means of bi-supported longitudinal flexure test with its hull loaded uniformly with steel weights. Fourteen strain gauges were bonded on the boat hull with their locations determined by a previous numerical model. A numerical model was developed using the finite element method software ANSYS® to simulate the same conditions of the bi-supported longitudinal flexure test. The strains read on each strain gauge were compared with the strains predicted at the corresponding locations in the numerical model. The experiments with the small-sized boat were conducted

primarily to validate the numerical simulations. The main objective was to compare experimental data with computational results. However, the numerical model can be extended to evaluate full-scale designs, including boats of slightly larger size with increased passenger capacity, based on the same methodology.

2. MATERIALS AND METHODS

This section presents the methodologies for prototype fabrication, mechanical characterization of the materials used, and the instrumentation and numerical modeling of the scaled-down vessel built for this study. The materials used were jute fiber, epoxy resin, and miriti wood. The characterization focused on green composite panels made of epoxy matrix reinforced with jute fibers. The properties of miriti were obtained from the literature.

2.1. Prototype building

The prototype built is a 730 mm-long boat with four layers of epoxy resin reinforced with unidirectional jute fiber fabric, in a mass ratio of 17% (resin) to 83% (fiber). Initially, a boat made of miriti was built. On this boat, the sandwich lamination was used and four layers of epoxy resin reinforced with jute fiber were bonded on the surfaces of the boat: two layers inside and two layers outside. On each side, the two layers of jute had the fiber oriented both transversally and longitudinally. Figure 2 shows the miriti boat, the lamination process with its directions and the prototype after the lamination. This sandwich structure has shown a good final quality, with a smoother surface aspect, full impermeability and no visible discontinuities on the lamination. In our previous work [9], the first prototype was built and analyzed without miriti as a core material, and it exhibited numerous discontinuities and leaks during flotation tests.

2.2. Characterization using DIC technique

The 3D Digital Image Correlation (DIC) technique provides complete deformation fields in the areas of interest for the analyzed specimens [10]. This offers important advantages in the characterization of certain materials, especially those with non-isotropic behaviors, such as some composite materials. The literature shows that it is common for composites to exhibit, for example, different properties in tensile and compressive states [11].

The analyses employed the stereoscopic Digital Image Correlation (DIC) technique, that is, using two cameras, which provides more accurate measurements [11]. Point Grey GRAS-50S5M/C (5 MP) photographic sensors and Tamron SP AF 180 mm F/3.5 macro lenses were used, suitable for the size of the measurement zones. The VIC 3D software by Correlated Solutions was used for system calibration and strain calculation. More details about the calibration methodology of the stereoscopic image acquisition and processing system should be found in [11]. Figure 3 shows the image acquisition system and the test setup: the load application device with a specimen already in place, the load cell (0 to 1 kN), and the data acquisition unit for the cell, model D4 from Vishay.

In this work, the methodology established in [12] and in the ASTM D-2344 Standard [13] were applied to perform three-point flexural bending tests on composite beams. Figure 4 shows the test bench including the gap between the supporting pins and the specimen, which has been prepared with a painting pattern for the application of the DIC technique. The applied load to strains obtaining was 100 N.

Three specimens were constructed with eight layers of unidirectional jute fabric each. The layers were arranged alternately at 0 and 90 degrees to the fiber direction. Each specimen measured 40 mm in length, 6.18 mm in width, and 6.49 mm in height.

Figure 5 shows an example of a strain field in the *x*-direction, along with the lines where the results were obtained for calculating the mechanical properties. The region selected are between the supports and the point

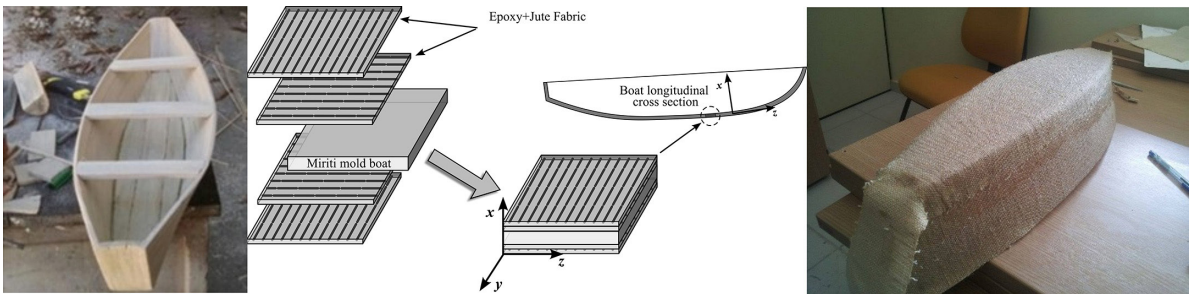

Figure 2: Manufacturing process steps: (Left) miriti boat mold; (center) sandwich lamination; (Right) final prototype.

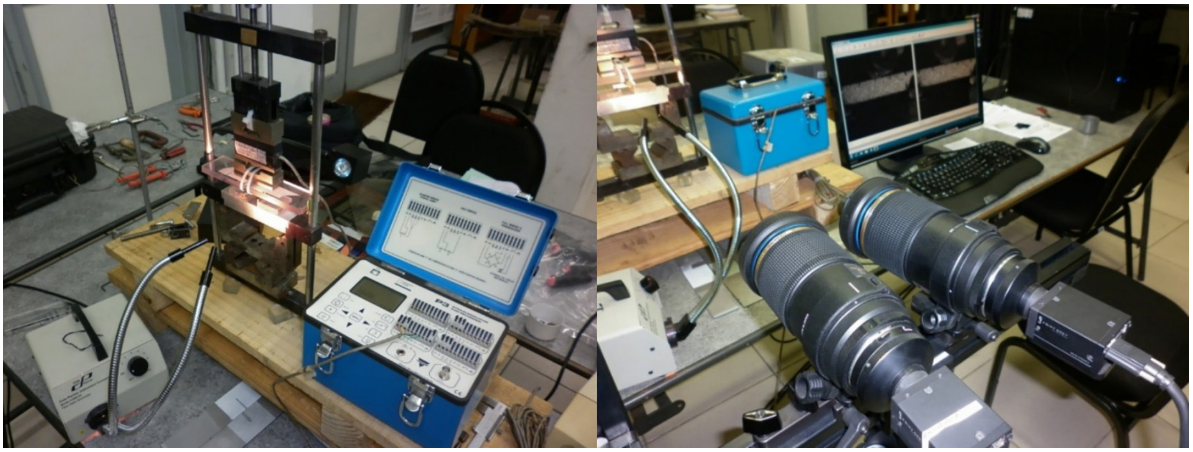

Figure 3: Experimental apparatus. Left: bending load application device, load cell and load acquisition and display equipment; Right: Image acquisition system for 3D DIC analysis, with macro lenses.

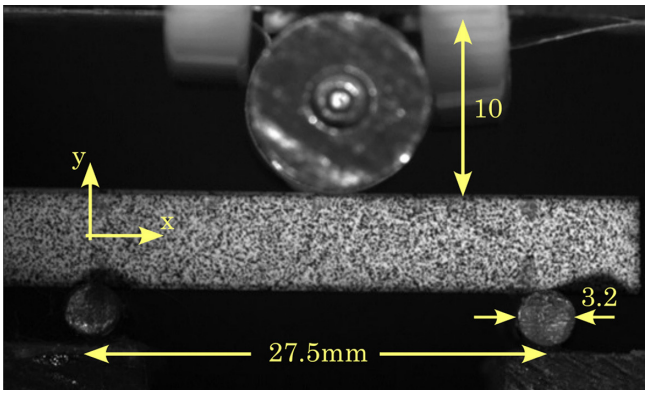

Figure 4: Three-point bending test setup showing the specimen under load: The force is applied through the central roller, while the two support points are spaced 27.5 mm. The coordinate system indicates the *x* and *y* directions.

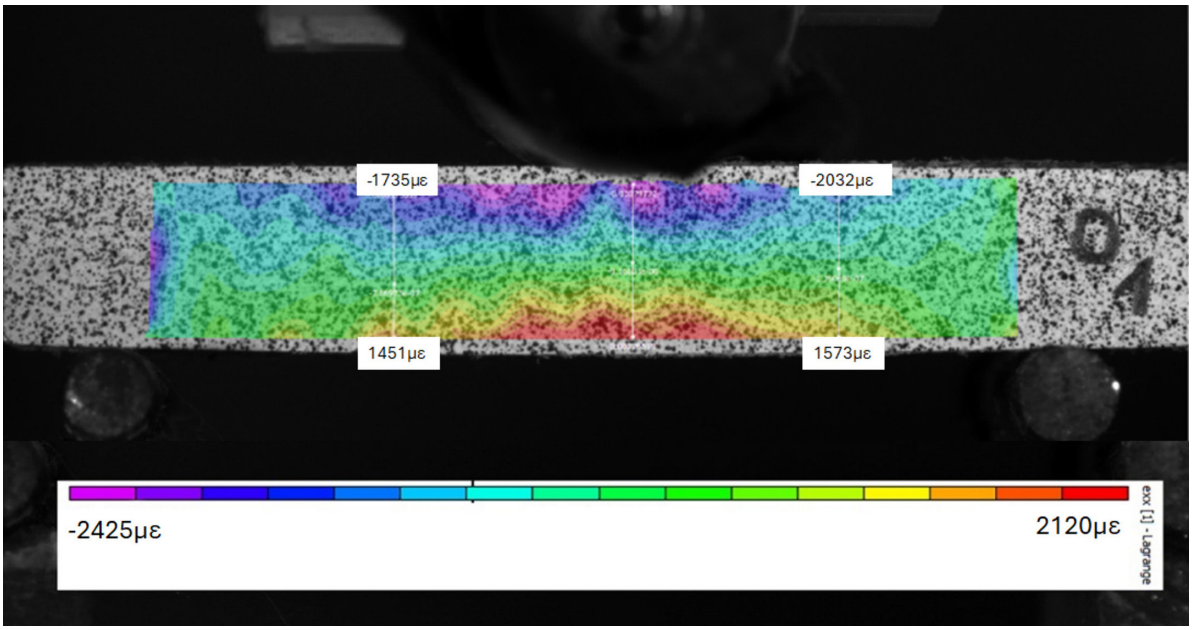

Figure 5: Normal strains field in the *x*-direction for a 100 N load.

of load application to avoid the effects of contact stresses. Deformation field for strains ε_{yy} and γ_{xy}, similarly to the one shown were also obtained for each specimen.

In the results and discussion section, strain graphs obtained from the measurements in the conducted tests will be presented, along with a table containing the properties derived from the information in these graphs.

3. EXPERIMENTAL ANALYSIS

The boat was subjected to a simple bending test, as the composite materials were distributed far from the neutral bending line, the boat has a high stiffness. With this high stiffness, testing in water would not produce significant strains in the boat's hull.

3.1. Experimental bending test setup

To obtain experimental data for validating the numerical model, a simple evaluation of flexure was conducted. The boat was supported along its longitudinal edges, and a load was applied inside it. The boat was instrumented with 14 strain gauges as shown in Figure 6. Strain gauges are the most widely used sensors for measuring deformations due to their high precision and are used in various types of structural assessments and stress analyses, such as in [14]. The strains values were measured by the data acquisition conditioner VISHAY® D4 and by EMEME EA-062AP-120 strain gages with the gauge factor of 2.05. Figure 6 also shows the boat with the bonded strain gauges and their connection to the acquisition system. Regarding strain measurement accuracy, we consider the error to be below 1%, consistent with the specifications provided by gage manufacturers, to ideal condition of application and acquisition. The test procedures also follow the guidelines presented in [15].

To load the boat, individual masses of 5kg were used. These box-shaped masses were placed on four supports in the center of the boat and represent the force applied when a person is standing or siting inside the boat. After each mass was added, the strains were measured. The last mass placed inside the boat was 4.2 kg, so the maximum load applied was 29.2 kg. Figure 7 shows the boat with an internal load of 10 kg and the supports used to distribute the load on the hull.

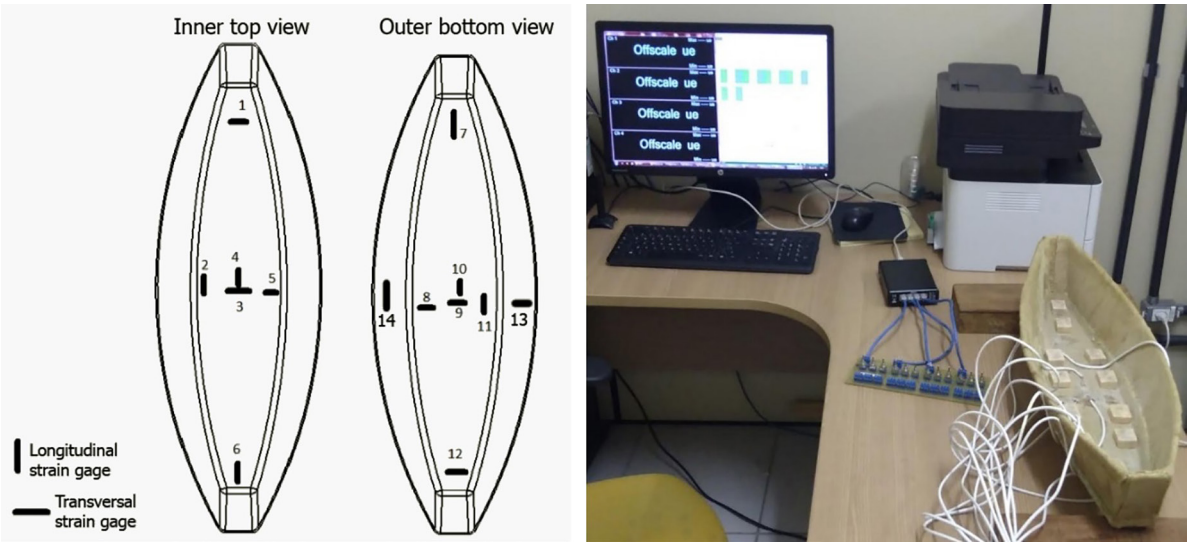

Figure 6: Prototype test: strain gauges positions (left), boat instrumented and connected to acquisition (right).

Figure 7: Internal loads and supports: internal load of 10 kg (left) load supports (right).

3.2. Numerical modeling

The boat geometry was designed using CAD software and then imported into ANSYS® Workbench [16], for a static structural analysis. To reduce computational cost and time, one quarter of the boat was evaluated, and symmetry boundary conditions were applied.

For the mechanical properties of miriti, two references were used. In first [17] provides data for the Young's Modulus and the second [18] is a handbook with the mechanical properties of various woods types. Based on these references for miriti wood, a Young's Modulus of 50 MPa and Poisson's ratio of 0.34 were considered in numerical simulations.

The SOLID187 3D element was used in the mesh. This element has 10 nodes with quadratic displacement, ideal for modeling irregular meshes. Each of its 10 nodes has three degrees of freedom (translations in *x*, *y*, and *z* directions) and supports plasticity, hyperelasticity, stress stiffening, large deflection, large strain, and a mixed formulation for nearly incompressible elastoplastic and fully incompressible hyperelastic materials [19]. The element size for jute composite was set as 5 mm and for miriti as 25 mm. The number of nodes and elements are respectively 352,461 and 212,659. In addition, a new coordinate system was created with the *y*-direction going towards the walls of the boat. Figure 8 shows the coordinate systems and the mesh.

For the boundary conditions, *frictionless supports* were used on the symmetrical faces and to avoid rigid body motion, a *displacement* constraint was applied at the interior edge of the boat. For the load, a force equal to one fourth of the weight of the load was applied to the same area used for the support. Figure 9 shows the boundary conditions used for this analysis.

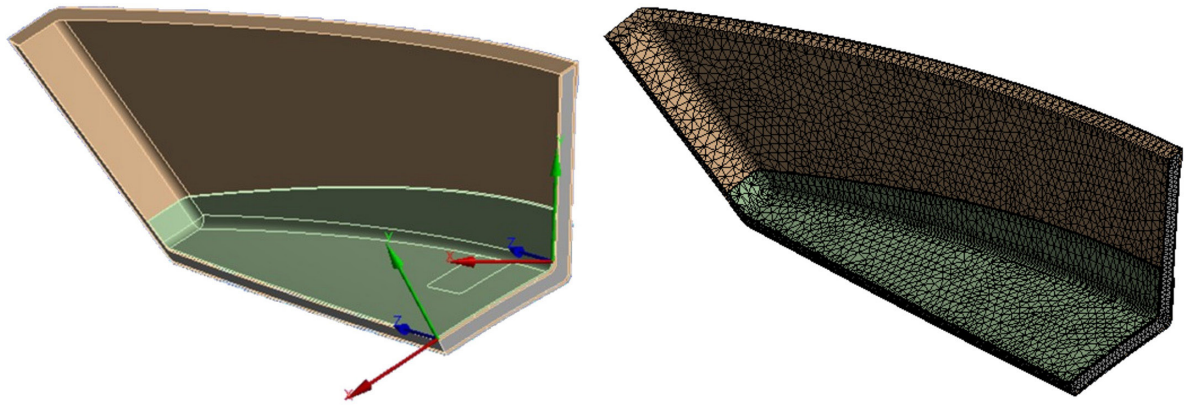

Figure 8: Coordinate systems used to extract the data (left) and finite element mesh used in simulations (right).

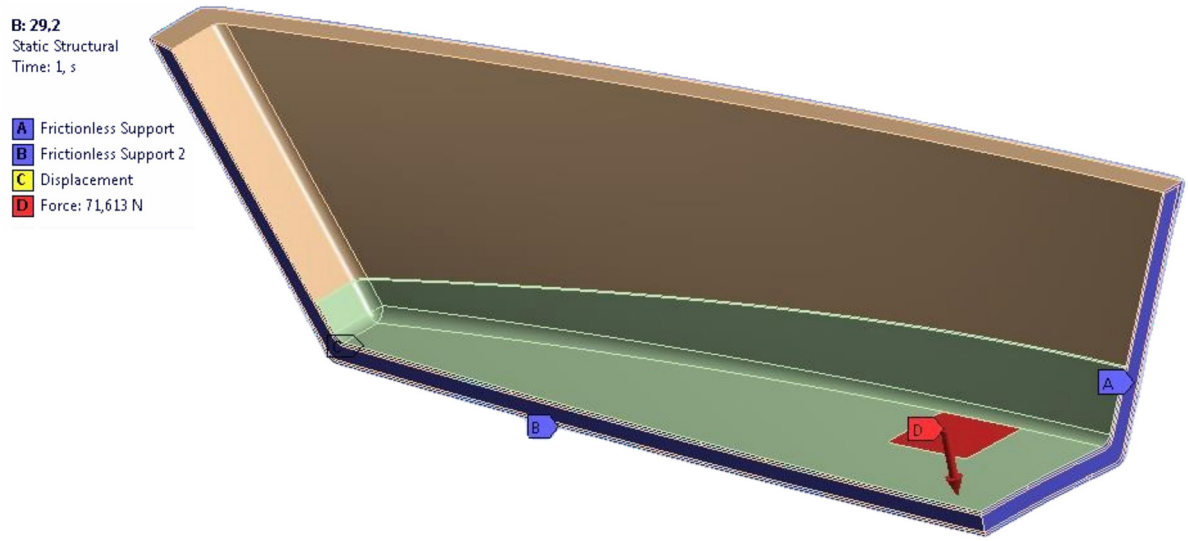

Figure 9: Boundary conditions applied to geometry model.

Table 1: Mechanical properties of the composite obtained from the bending test.

SPECIMEN	TENSILE MODULUS (GPa)	COMPRESSIVE MODULUS (GPa)	SHEAR MODULUS (GPa)	POISSON'S RATIO
#1	7.41	5.51	3.88	0.40
#2	9.93	5.87	5.53	0.34
#3	8.79	7.77	6.21	0.31
Mean Value	**8.57**	**6.37**	**5.48**	**0.36**

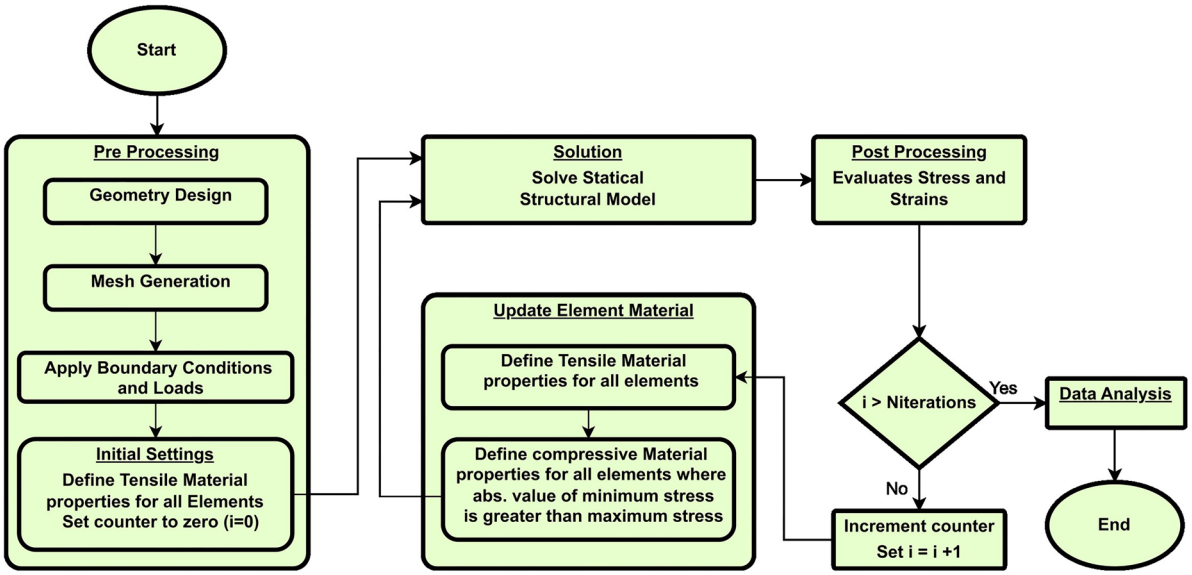

Figure 10: Flowchart of numerical solution for bimodular materials in ANSYS.

As shown in Table 1, the jute composite exhibits anisotropic behavior, with distinct mechanical properties under tensile and compressive stresses, resulting in a 35% difference between the two. This difference proved significant, leading to unacceptable discrepancies between the experimental and numerical results in the initial modeling, as standard ANSYS Workbench setup does not allow for separate behaviors under tension and compression. To address this issue, a code was developed in ANSYS Parametric Design Language (APDL) [20] to correctly model the behavior of the jute composite. Basic setup of this code can be found in [20]. This code identifies elements under compressive stress and assigns them specific material properties. This process is applied to each component in the model, requiring a unique element type for each. Figure 10 illustrates the flowchart of the APDL code, where black arrows represent the initial configurations, and the red arrow indicates the second configuration.

4. RESULTS AND DISCUSSION

4.1. Mechanical properties obtaining with DIC

4.1.1. Modulus of elasticity

Figure 11 shows the normal strains in *x*-direction for one specimen, measured along the lines to left and right of the load application point (as indicated in Figure 4). The strains are plotted as function of *y*-distance in the reference coordinate system, along with the best-fit linear equation.

It is worth noting the reasonably linear behavior of the deformations, as well as the close agreement between the observed values. The coefficients of the linear fit equations of the deformation curves (such as those shown in Figure 11) are applied in Equation 1:

$$\varepsilon_{xx}(y) = -ky - b \tag{1}$$

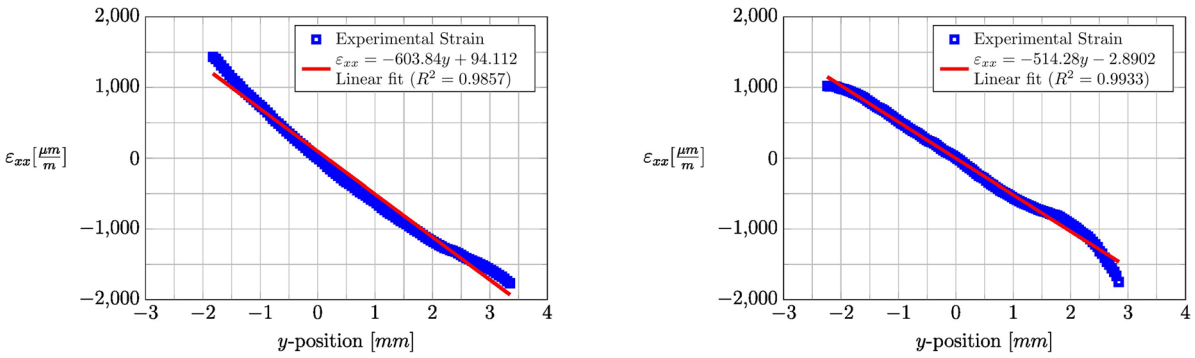

Figure 11: Variations of normal strains (ε_{xx}) with respect to the beam y position: (left) in the left of the load and (right) right of the load application.

where y is the coordinate in the height direction, with its origin at the geometric center of the specimen's height, k is the slope of the linear fit for the measured points, and b is its intercept. By applying the force and moment equilibrium equations, Equation 2 can be derived to calculate the tensile and compressive moduli.

$$E_{T,C} = \frac{M}{k \cdot l \cdot (1 \mp a^2)}, \text{ where } a = \frac{2}{h}\frac{b}{k} \tag{2}$$

here, M is the bending moment in the region of interest, h is the height of the specimen, and I is the transverse moment of inertia. The parameter $\frac{b}{k}$ represents the offset between the neutral axis and the centroid of the section. It is proportional to the difference between the tensile and compressive moduli. The results for the moduli are presented at the end of this section in Table 1.

4.1.2. Poisson's coefficient

To calculate the Poisson's ratio, the same procedure applied to the strains in the x-direction was used for the strains in y-direction. That is, linear equations were defined to represent the behavior of these strains along the beam height. The slope of the fitted line for ε_{yy} was divided by the slope of the fitted line for ε_{xx}, thus defining the material's Poisson's ratio. Figure 12 shows the graphs of normal strains ε_{yy} as a function of y-position, both to the right and left of the load application. Their corresponding approximate representative equations are also presented.

Similar to the behavior observed in the ε_{xx} strains, the ε_{yy} strains also exhibited a highly linear trend, further validating the accuracy and reliability of the measurements.

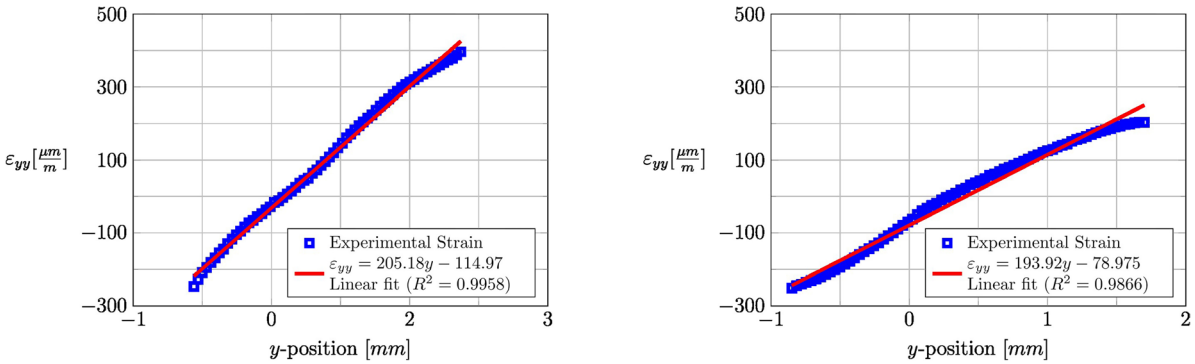

Figure 12: Variations of normal strains (ε_{yy}) with respect to the beam's y-position: (left) to the left ot the load and (right) to the right of the load application.

4.1.3. Shear modulus

The shear modulus (G_{xy}) was determined from the slope of the linear portion of the shear stress (T_{xy}) vs. shear strain (γ_{xy}) graphs along the height of the measurement section. The (γ_{xy}) values were obtained from measurements, while the τ_{xy} was calculated using y as well as γ_{xy} using Equation 3.

$$\tau_{xy} = \frac{3P}{4A}\left[1-\left(\frac{2y}{h}\right)^2\right] \tag{3}$$

Where A is the cross-sectional area. Figure 13 shows the shear stresses distribution along the γ_{xy}, on both the left and right sides of the load application. Although the linear trend is less apparent when compared with the observed in Figure 11 and Figure 12, the R^2 values remain above 0.95. Transverse modulus is obtained from the slope of the linear fit curve.

Table 1 presents a summary of the computed mechanical properties for the tested specimen obtained with the DIC technique. The difference observed in the material's stiffness in tension and compression indicates its anisotropic nature. The values obtained confirm the expected mechanical performance of the composite, reinforcing its potential for structural applications. The average values from Table 1 were used as input data in the numerical model.

4.2. Numerical and experimental results

During the test all the strain gauges performed well, the strains remained constant for each load and there were no significant variations over time for the same load. In Figures 14, 15 and 16, it is shown a comparison between the numerical and the experimental strains in the positions described in Figure 6. In these figures, the abscissa axis represents the load in kilograms, while the ordinate axis is the strain in με.

It is noteworthy that, in most cases, the numerical and experimental strain values are nearly identical. However, exceptions were observed at points 9 and 12. These discrepancies can be attributed to slight differences between the geometry of the numerical model and the actual boat. Variations in material distribution, such as areas with excess or insufficient material, can cause certain regions to exhibit either increased or reduced rigidity. Despite these differences, the numerical model performed as expected, as both tensile and compressive behaviors were consistent at each point when comparing the numerical and experimental results.

Figure 17 shows the longitudinal and transversal strains along the outer longitudinal centerline, as obtained from the numerical model. A clear similarity can be observed in the strain patterns, with both transverse and longitudinal strains exhibiting the same behavior. The only difference lies in their magnitudes, which is expected since the load conditions remain constant, and the only variable is the weight inside the boat. The higher longitudinal strain values found at the end of the centerline can be attributed to the contact surface between the supports and the longitudinal edges of the boat's hull.

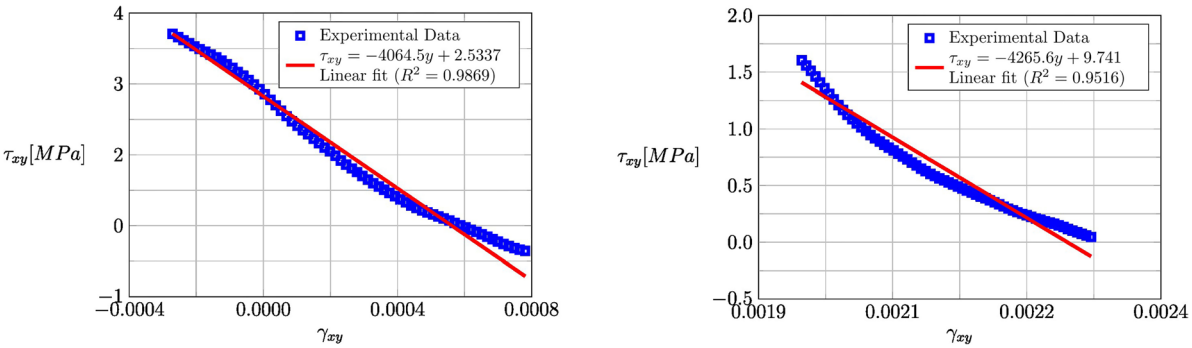

Figure 13: Variations of shear stress with respect to the shear deformation: (left) to the left of the load and (right) to the right of the load application.

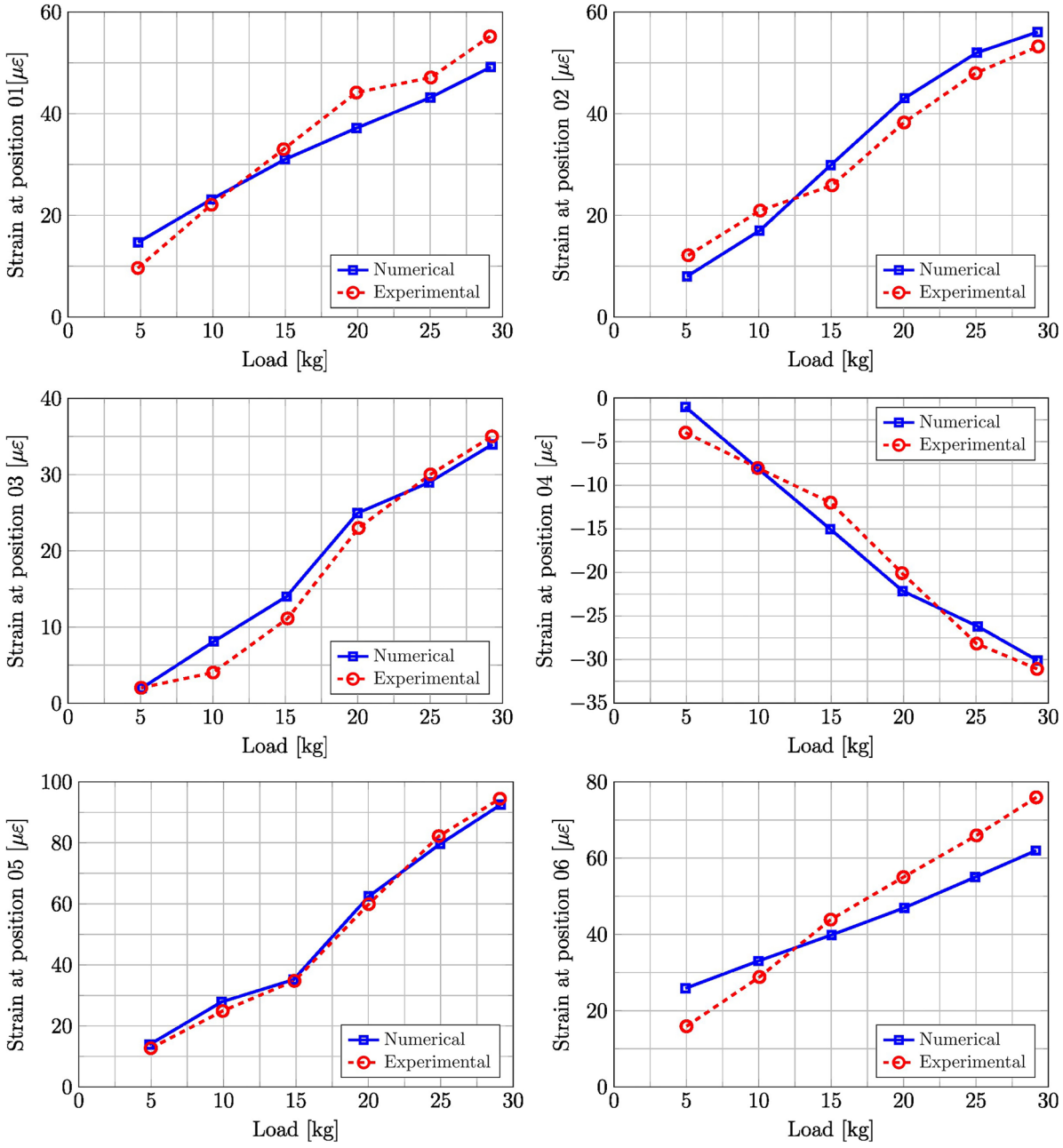

Figure 14: Experimental and numerical results for inner measurements (strain gauge positions 01–06).

In Figure 18, results of normal stresses distributions along the boat hull are presented for the maximum load applied. These results indicate low magnitudes of stresses with maximum values of approximately 7 MPa, well below the strength limit of the jute composite which is around 70 MPa [21]. The boat weighs only 0.945 kg and can effortlessly suport loads up to 30 kg. So, the safety factor to this application is around 10. Evidently, to scale up this boat to a real size application, when the load and bending stresses are higher, a thicker miriti wood and more jute layers could be added, to comply with safety standards. This highlights the potential of jute fiber composites for small boat construction.

5. CONCLUSIONS

In this work, a sandwich-structured boat with a miriti core and an epoxy resin coating reinforced with jute fiber was subjected to experimental and numerical flexure tests. The experimental tests were monitored by 14 strain

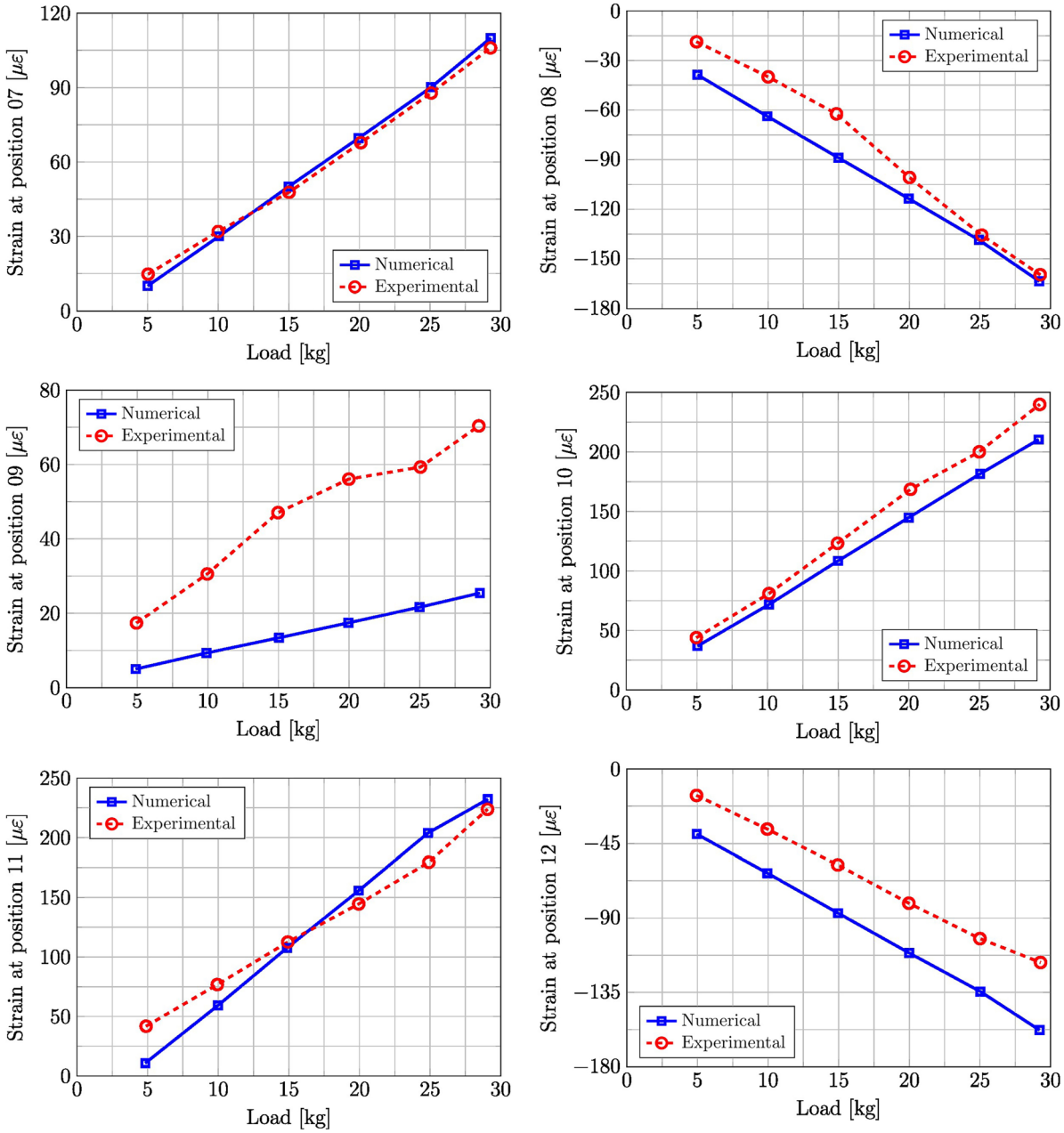

Figure 15: Experimental and numerical results for outer measurements (strain gauge positions 07-12).

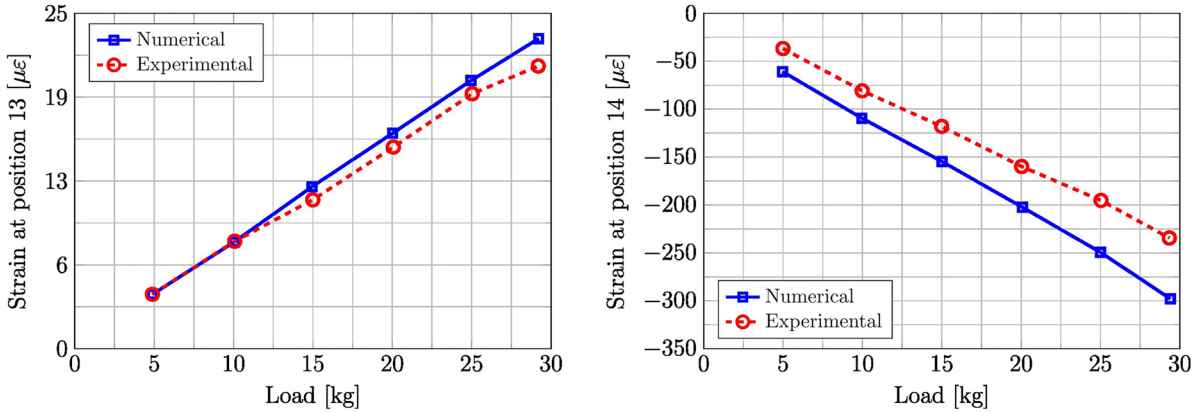

Figure 16: Experimental and numerical strains at the lateral outer wall (strain gauge positions 13-14).

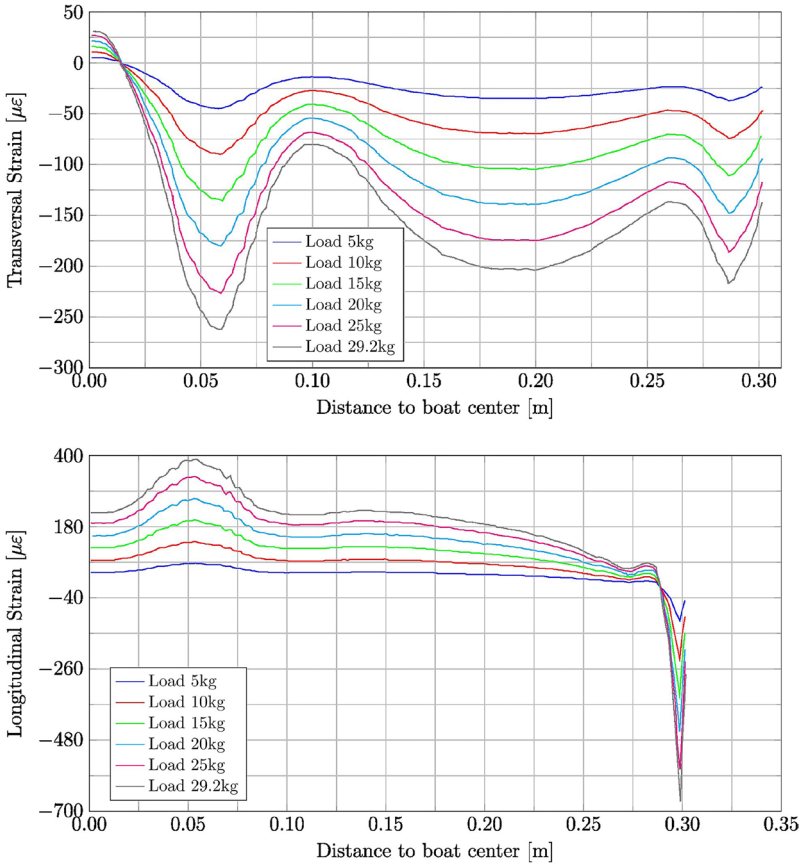

Figure 17: Transversal and longitudinal strains along the outer longitudinal line of the boat obtained from the numerical model.

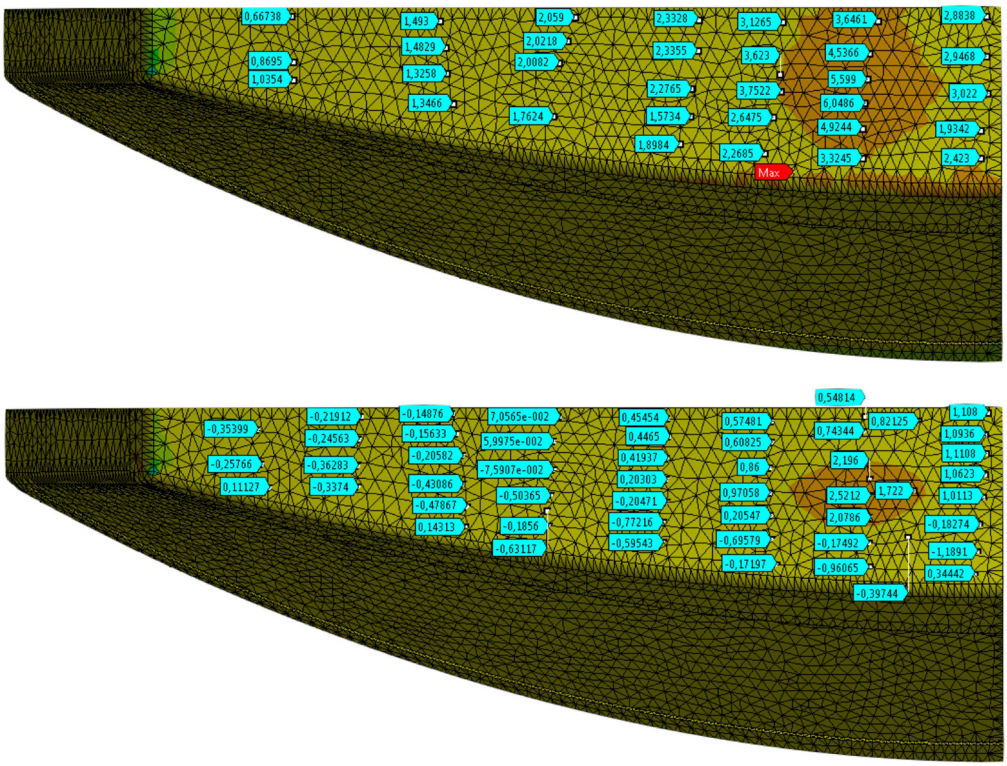

Figure 18: Normal stresses [MPa] at boat hull along: (top) *z*-axis (bottom) *x*-axis.

gauges. The primary objective of this work was to validate the numerical model for evaluating the behavior of the sandwich structure, accounting for the anisotropy properties of the jute composite.

For a more comprehensive characterization of the jute fiber composite with epoxy resin, bending tests were conducted by measuring the strain using the DIC technique. This approach allowed the determination of the elastic properties in different planes, providing more accurate input for the numerical model to deal with the orthotropy of the material, including its distinct behaviors under tension and compression.

The average error found between the numerical model results and the experimental results at the fourteen points analyzed was 12.7 $\mu\varepsilon$, with two points showing much higher errors than the others, namely points 9 and 12, which presented average errors of 31.4 $\mu\varepsilon$ and 30.34 $\mu\varepsilon$, respectively. This was possibly due to localized lamination issues that may have caused punctual reductions in stiffness, since the deformations in the experimental model were greater than those in the numerical one, although they followed the same behavioral trend. Excluding these two points from the analysis, the average error for the remaining twelve points was 9.66 $\mu\varepsilon$.

The close agreement between strain gage measurements and numerical results at most points confirms that the main objective was achieved. This validates the numerical methodology, which now can used to full-scale models, including fluid-structure interaction, with greater reliability and aiding in the design of small boats using these innovative materials.

6. ACKNOWLEDGMENTS

The authors thank the UFPA Extension Office for financial support.

7. BIBLIOGRAPHY

[1] O GLOBO, "Os Ribeirinhos no Amazonas", https://oglobo.globo.com/brasil/os-ribeirinhos-no-amazonas-14624351, acessado em janeiro de 2025.

[2] RIBEIRO, J.L.P., GREGORI, M.L., PARDINI, L.C., "Prediction of elastic properties of thermo structural composites with multidirectional reinforcement", *Matéria*, v. 13, pp. 33–48, 2008. http://doi.org/10.1590/S1517-70762008000100005.

[3] ASHBY, M.F. Materials and the environment: eco-informed material choice, Oxford, UK, Butterworth-Heinemann, 2012. http://doi.org/10.1016/C2010-0-66554-0

[4] CRUPI, V., EPASTO, G., NAPOLITANO, F., *et al*., "Green composites for maritime engineering: a review", *Journal of Marine Science and Engineering*, v. 11, n. 3, pp. 599, 2023. http://doi.org/10.3390/jmse11030599.

[5] SURIANI, M.J., ILYAS, R.A., ZUHRI, M.Y.M., *et al*., "Critical review of natural fiber reinforced hybrid composites: processing, properties, applications and cost", *Polymers*, v. 13, n. 20, pp. 3514, 2021. http://doi.org/10.3390/polym13203514. PMid:34685272.

[6] OLIVEIRA, P.R., MAY, M., PANZERA, T.H., *et al*., "Bio-based/green sandwich structures: a review", *Thin-walled Structures*, v. 177, pp. 109426, 2022. http://doi.org/10.1016/j.tws.2022.109426.

[7] MISRI, S., LEMAN, Z., SAPUAN, S.M., *et al*., "Mechanical properties and fabrication of small boat using woven glass/sugar palm fibres reinforced unsaturated polyester hybrid composite", *IOP Conference Series. Materials Science and Engineering*, v. 11, pp. 012015, 2009. http://doi.org/10.1088/1757-899X/11/1/012015.

[8] BARROS, M.A.S. Vantagens da aplicação de material compósito em substituição as ligas metálicas na aviação. Tese de M.Sc., Universidade Federal do Pará, Belém, Pará, 2014.

[9] CARVALHO, M.F., XAVIER, M.A., VALENTE, J.C.F., *et al*., "Use of green composites for manufacturing small boats in the Amazon: numerical and experimental evaluations", *Matéria*, v. 22, n. 2, pp. 1–11, 2017. http://doi.org/10.1590/s1517-707620170002.0160.

[10] GONZÁLES, G.L.G., RODRIGUES, L.D., MEGGIOLARO, M.A., *et al*. "Strains in shallow and deep notches using two dic algorithms", In: Jin, H., Yoshida, S., Lamberti, L., Lin, MT. (eds), *Advancement of optical methods in experimental mechanics*, Volume 3, Cham, Springer, 2016. http://doi.org/10.1007/978-3-319-22446-6_35.

[11] RODRIGUES, L. D., "Aplicação da técnica DIC a espécimes com diferentes formas, materiais e gradientes de deformação". D.Sc. Thesis, Pontifícia Universidade Católica do Rio de Janeiro, Rio de Janeiro, 2014.

[12] MAKEEV, A., HE, Y., CARPENTIER, P., *et al*., "A method for measurement of multiple constitutive properties for composite materials", *Composites. Part A, Applied Science and Manufacturing*, v. 43, n. 12, pp. 2199–2210, 2012. http://doi.org/10.1016/j.compositesa.2012.07.021.

[13] AMERICAN SOCIETY FOR TESTING AND MATERIALS, ASTM D 2344/D 2344M Standard Test Method for Short-Beam Strength of Polymer Matrix Composite Materials and Their Laminates, West Conshohocken, ASTM, 2006.

[14] RODRIGUES, L.D.; FREIRE, J.L.; VIEIRA, R.D., "Development and experimental evaluation of a new technique for the measurement of residual tensions", *Matéria*, v. 16, pp. 842–856, 2011. http://doi.org/10.1590/S1517-70762011000400006.

[15] AMERICAN SOCIETY FOR TESTING AND MATERIALS, ASTM D6856/D6856M-03 Standard Guide for Testing Fabric-Reinforced "Textile" Composite Materials, West Conshohocken, ASTM, 2016.

[16] ANSYS Inc., ANSYS Workbench, Release 18.2 User's Guide, Canonsburg, PA: ANSYS Inc., 2017.

[17] SANTOS, L.F.G. "Estudo sistemático do Miriti (Mauritia flexuosa) para o desenvolvimento de ECO-VANT". Tese de M.Sc., Universidade Federal de Ouro Preto, Ouro Preto, Minas Gerais, 2016.

[18] SENALIK, C.A., FARBER, B., "Mechanical properties of wood", In: Green, D.W., Winandy, J.E., Kretschmann, D.E. (eds), Wood handbook: wood as an engineering material. Madison, WI, USDA Forest Service, Forest Products Laboratory, 1999.

[19] ANSYS Inc., ANSYS Mechanical APDL Element Reference, Release 18.2, Canonsburg, PA: ANSYS Inc., 2017.

[20] ANSYS Inc., ANSYS Parametric Design Language Guide, Release 15.0, Canonsburg, PA: ANSYS Inc., 2013.

[21] KUWAHARA, M. Compósitos de poliéster reforçados por fibras de bambu e sisal: características mecânicas e aspectos fratográficos. Tese de M.Sc., Universidade Federal do Pará, Belém, Pará, 2013.